Clinical Imaging 61 (2020) 20–26

Contents lists available at ScienceDirect

Clinical Imaging

journal homepage: www.elsevier.com/locate/clinimag

Body Imaging

Optimizing b-values for accurate depiction of pancreatic cancer with tumor-associated pancreatitis on computed diffusion-weighted imaging

Koji Tokunaga[a], Shigeki Arizono[a,*], Hironori Shimizu[a], Koji Fujimoto[a], Mariyo Kurata[b], Sachiko Minamiguchi[b], Hiroyoshi Isoda[a], Kaori Togashi[a]

[a] Department of Diagnostic Imaging and Nuclear Medicine, Kyoto University Graduate School of Medicine, 54 Kawaharacho, Shogoin, Sakyo-ku, Kyoto 606-8507, Japan
[b] Department of Diagnostic Pathology, Kyoto University Graduate School of Medicine, 54 Kawaharacho, Shogoin, Sakyo-ku, Kyoto 606-8507, Japan

ARTICLE INFO

Keywords:
Pancreatic cancer
Magnetic resonance imaging
Diffusion-weighted imaging
Computed diffusion-weighted imaging
Tumor-associated pancreatitis

ABSTRACT

Purpose: To determine the optimal b-value for accurate depiction of pancreatic cancer (PC) in patients with active tumor-associated pancreatitis (TAP), using computed diffusion-weighted imaging (cDWI) with a range of b-values up to 3000 s/mm^2.

Methods: The study protocol was approved by the institutional review board. We retrospectively analyzed 34 consecutive PC cases with active TAP who underwent pancreatectomy without preoperative therapy. Four cDWI datasets with b-values of 1500–3000 s/mm^2 (cDWI$_{1500}$–cDWI$_{3000}$) were generated from the original DWI datasets with b-values of 0 and 1000 s/mm^2 obtained using a 3-T scanner. Two board-certified radiologists evaluated images qualitatively (tumor conspicuity and total image quality), and another two board-certified radiologists placed regions of interest for quantitative evaluations (apparent diffusion coefficient [ADC] values of both lesions, contrast ratio [CR] of PC to active TAP, and volume ratio [VR] of PC to surgical specimen).

Results: As the b-value increased, tumor conspicuity improved significantly in cDWI$_{2000}$ and cDWI$_{2500}$ (P = 0.0121 and 0.0015, respectively), although total image quality decreased in all cDWIs compared with DWI$_{1000}$ (P < 0.0001). Significantly lower ADC values were seen in PC (P < 0.0001). All cDWI groups showed positive correlation between the tumor conspicuity and ADC difference between PC and TAP. CR increased with the b-value, while VR decreased. Significant equivalence of VR to the surgical specimen was seen on cDWI$_{2000}$ (P = 0.0031).

Conclusion: Accurate depiction of PC was optimal with cDWI$_{2000}$ in the presence of active TAP.

1. Introduction

Pancreatic cancer (PC) is a common, highly aggressive malignant neoplasm. The incidence of PC has been increasing over the years [1]. Recognizing the borders of the cancer is important, particularly when discussing resectability, deciding on surgical procedures, planning radiotherapy, or evaluating therapeutic responses to chemoradiotherapy or chemotherapy [2–6]. Clinically, multimodal imaging techniques utilized for this task include ultrasonography, computed tomography (CT), and magnetic resonance imaging (MRI) [7].

The utility of diffusion-weighted imaging (DWI) with a high b-value range (b = 800–1000 s/mm^2) has been reported for several malignancies, including PC [8–12]. The b-value is an arbitrary parameter set when performing DWI, which is determined by the amplitude, the duration of the applied gradients, and the interval between the two gradients [13]. Delineating the borders of the tumor mass becomes difficult in patients with PC and tumor-associated pancreatitis (TAP) of the upstream pancreatic parenchyma on DWI, because both lesions demonstrate high signal intensity (SI) on DWI [9,14], especially when the TAP is in the acute or active inflammatory phase (active TAP), as this phase lowers the apparent diffusion coefficient (ADC) value in contrast to the chronic, inactive or less active inflammatory phase [11,15,16]. TAP may occur in approximately 17% of PC patients [17]. Higher b-value-based DWI with b > 1200 s/mm^2 is helpful to visualize PC in these cases [18]. However, image deterioration is seen in higher b-value-based DWI, due to the decrease in signal-to-noise ratio and the associated distortion, especially in the abdomen [19,20].

Computed DWI (cDWI) is a technique for generating DWI with any

* Corresponding author.
E-mail addresses: tokunaga.koji.28m@kyoto-u.jp (K. Tokunaga), arizono@kuhp.kyoto-u.ac.jp (S. Arizono), hshimizu@kuhp.kyoto-u.ac.jp (H. Shimizu), kfb@kuhp.kyoto-u.ac.jp (K. Fujimoto), mariyo@kuhp.kyoto-u.ac.jp (M. Kurata), minami@kuhp.kyoto-u.ac.jp (S. Minamiguchi), sayuki@kuhp.kyoto-u.ac.jp (H. Isoda), ktogashi@kuhp.kyoto-u.ac.jp (K. Togashi).

https://doi.org/10.1016/j.clinimag.2020.01.007
Received 7 June 2019; Received in revised form 5 December 2019; Accepted 7 January 2020

b-value from at least two different b-value-based DWIs [21]. Using a cDWI-generating program, cDWI can be generated automatically and very easily within a few minutes without any expertise. Such programs can be created by radiologists, and are also available in some open-source image analysis software [22]. The utility of cDWI for detecting PC has been reported [23]. However, the utility of cDWI remains unclear for border delineation between PC and TAP, especially in PC patients with active TAP. Optimal b-values for cDWI in such patients remain unclear.

We sought to evaluate the utility of cDWI and determine optimal b-values for the accurate depiction of PC in patients with active TAP, using cDWI with a broad range of b-values up to 3000 s/mm^2.

2. Material and methods

2.1. Patients

This study protocol was approved by the institutional review board prior to initiation of the study, and the need to obtain written informed consent was waived owing to the retrospective nature of the study. The following patients were included: 1) patients who underwent abdominal MRI prior to therapy for histologically diagnosed PC between January 1, 2011 and March 31, 2017; 2) patients who were diagnosed clinically and radiologically with active TAP; and 3) patients who underwent radical pancreatectomy ≤30 days after MRI. The following patients were excluded: 1) patients who received preoperative therapy; 2) patients who were under treatment for another malignant tumor; and 3) patients who had pancreatitis associated with endoscopic retrograde cholangiopancreatography based on the medical record.

The presence of active TAP was confirmed with triple-phase contrast-enhanced CT (CECT) obtained ≤2 weeks before the MRI study, based on well-documented criteria used in the literature [24,25], and elevations of amylase or lipase from the reference range in our institution (amylase, 45–140 U/L; lipase, 11–53 U/L) ≤2 weeks before the MRI study.

2.2. MRI protocol

All MRI examinations were performed using a 3.0-T MR system (Magnetom Prisma® or Magnetom Skyra®; Siemens Healthineers, Erlangen, Germany) equipped with spine matrix and body matrix coils. DWIs were obtained in single-shot spin-echo (SE) echo-planar imaging (EPI) sequence in the axial plane with free breathing and respiratory triggering using the Prospective Acquisition CorrEction (PACE) technique to correct for respiratory motions. Imaging parameters were as follows: repetition time, 1800 ms; echo time, 55 ms; field of view, 31.8 × 26.0 cm; matrix size, 86 × 128; 30 slices; slice thickness/gap, 5/1 mm; spectral fat saturation; 4 averages; k-space-based parallel imaging technique (generalized autocalibrating partially parallel acquisitions) with an acceleration factor of 2; and b-values of 0, 500, and 1000 s/mm^2.

Baseline MR images, including a fat-saturated T2-weighted turbo spin-echo (TSE) sequence with respiration triggering using the PACE technique, a breath-hold heavily T2-weighted half-Fourier single-shot TSE sequence, a breath-hold T1-weighted gradient-echo (GRE) sequence with dual-echo of in- and opposed-phases, and MR cholangiopancreatography with breath-holding using a single-shot TSE sequence were acquired before administration of Gd-EOB-DTPA (Primovist®; Bayer Schering Pharma AG, Berlin, Germany). Pre-contrast, dynamic and delayed hepatocyte-phase T1-weighted three-dimensional spoiled GRE images in the axial plane were obtained using a volumetric interpolated breath-hold examination (VIBE) sequence with chemically selective fat saturation. After acquiring the initial VIBE sequence, a bolus of 25 μmol/kg body weight Gd-EOB-DTPA was injected and flushed with 40 mL of sterile saline solution at a rate of 2.5 mL/s into the antecubital vein. A power injector (Sonic Shot®; Nemoto-Kyorindo, Tokyo, Japan) was used for injection of contrast agent and saline. Arterial-, portal venous-, and equilibrium-phase images were acquired after bolus injection of Gd-EOB-DTPA with delay times of 25 s, 65 s, and 110 s, respectively. After the dynamic study, DWI was obtained, followed by hepatocyte-phase imaging at 20–25 min after injection of contrast agent [26].

2.3. Computed DWI

The SI on DWI exponentially attenuates with the b-value based on a measured ADC value [21]. cDWI is a technique to generate high b-value DWI by extrapolating decaying signal with DWI obtained from the actual scan [21]. Based on the following signal model, we calculated ADC values from the combination of b-values in two DWIs with b-values of 0 and 1000 s/mm^2, according to a previous study regarding the combination of b-values as material [27], with nonlinear least-squares fitting using commercial software (MATLAB R2013b®; The Math Works, Natick, MA) and generated cDWI with b-values of 1500, 2000, 2500, and 3000 s/mm^2 [28] using Eq. (1):

$$S_b = S_0 exp(-b \times ADC) \quad (1)$$

where S_b corresponds to the SI of a given b-value and S_0 corresponds to the SI without applying any diffusion gradients.

We adopted a noise-reducing concept assuming that pixels demonstrating a negative ADC represented noise and were excluded from the cDWI-generating algorithm and portrayed as zero-signal pixels [29].

2.4. Histopathology

The final diagnosis was confirmed by pathological examination of the surgical specimen. Two board-certified pathologists (M.K. and S.M., with 8 years and 24 years of experience, respectively) made the diagnoses separately and later reached a consensus decision. Each radically resected pancreas, fixed with 10% neutral-buffered formalin, was sent to the pathology laboratory. The resected pancreas was wholly sliced in the sagittal direction in 5-mm thickness. All slices were placed side by side and a digital photograph was taken. Slices were embedded in paraffin blocks, cut into 4-μm thicknesses, and stained with hematoxylin and eosin for pathological examination.

2.5. Qualitative evaluation

Qualitative assessment was performed by two board-certified radiologists (T.S. and S.K., with 8 and 9 years of experience in abdominal radiology) together with consensus on a commercially available medical image viewer (Aquarius NET Client Viewer®; TeraRecon, Foster City, CA) with reference to other MRI sequences such as T1-weighted, T2-weighted, and dynamic contrast enhanced T1-weighted images. Aside from knowing that the patients had both PC and active TAP, observers were blinded to the medical information of each patient including location and size of the tumor [9]. To minimize any reading bias, we randomized the order of patients before every session and scheduled a 2-week interval between interpretation sessions, with a total of 10 weeks for the evaluation period [26]. Results of cDWI with b-values of 1500, 2000, 2500, and 3000 s/mm^2 ($cDWI_{1500}$, $cDWI_{2000}$, $cDWI_{2500}$, and $cDWI_{3000}$) and DWI with a b-value of 1000 s/mm^2 (DWI_{1000}) were evaluated independently. Evaluation points were tumor conspicuity and total image quality. Tumor conspicuity and total image quality were scored on a 4-point scale as follows: 1, poor; 2, fair; 3, good; 4, excellent, for DWI and cDWI images from each case (Table 1, Fig. 1). Tumor conspicuity was scored based on the clarity of the tumor border and the difference in SI between PC and distal pancreatic parenchyma. Total image quality was comprehensively scored based on the degree of artifact, organ orientation, and image contrast.

Table 1
Scores for tumor conspicuity and total image quality

Scores	Tumor conspicuity	Total image quality
4	Definite border with clear difference in SI between PC and distal parenchyma	Good, very small artifact, very good contrast, very good orientation of the organs
3	Unclear border with clear difference in SI between PC and distal parenchyma	Fair, small artifact, good contrast, good orientation of the organs
2	Unclear border with small difference in SI between PC and distal parenchyma	Moderate artifact, slightly decreased contrast, slightly decreased orientation of the organs
1	Difficulty in PC visualization, or no difference in SI between PC and distal parenchyma	Poor, strong artifact, poor contrast, poor orientation of the organs

PC, pancreatic cancer; SI, signal intensity.

2.6. Quantitative evaluation

Quantitative analysis of DWI was performed together by another two board-certified radiologists (K.T. and S.A., with 10 and 17 years of experience in abdominal radiology) reaching a consensus decision, with no blinding to the patient's medical information including diagnosis and location of PC. Freehand regions of interest (ROIs) were drawn on all images (DWI_{1000}, $cDWI_{1500}$, $cDWI_{2000}$, $cDWI_{2500}$, and $cDWI_{3000}$), to include the largest area to be considered as the PC [30] and active TAP separately. Care was taken to exclude vessels, ducts, cystic lesions, and calcifications within the lesion [31]. Mean values of SI, ADC value, difference of ADC values between PC and active TAP (ΔADC), and area within the ROI (A_{DWI}) were measured in all cases. Contrast ratio (CR) of SI in PC to the TAP was calculated using the following Eq. (2):

$$CR = (SI_{PC} - SI_{TAP})/SI_{PC} \quad (2)$$

where SI_{PC} and SI_{TAP} represent mean SI within the ROI placed in each lesion.

The ΔADC was calculated using the following Eq. (3):

$$\Delta ADC = ADC\ value\ of\ active\ TAP - ADC\ value\ of\ PC \quad (3)$$

Volume of PC based on DWI (V_{DWI}) was calculated using the following Eq. (4):

$$V_{DWI} = \sum (A_{DWI} \times T_{DWI}) \quad (4)$$

where T_{DWI} stands for slice thickness on DWI.

Histopathological extent and geographic location of the PC were marked and hand-drawn in the hard copy of the digital photograph and a two-dimensional cancer map was created by the same two pathologists who made final diagnoses as a consensus decision (Fig. 2) [32]. Areas of the PC in the cancer map ($A_{Pathology}$) were measured using open access software (ImageJ; National Institutes of Health, Bethesda, MD). The volume of the PC from the cancer map ($V_{Pathology}$) was calculated using the following Eq. (5):

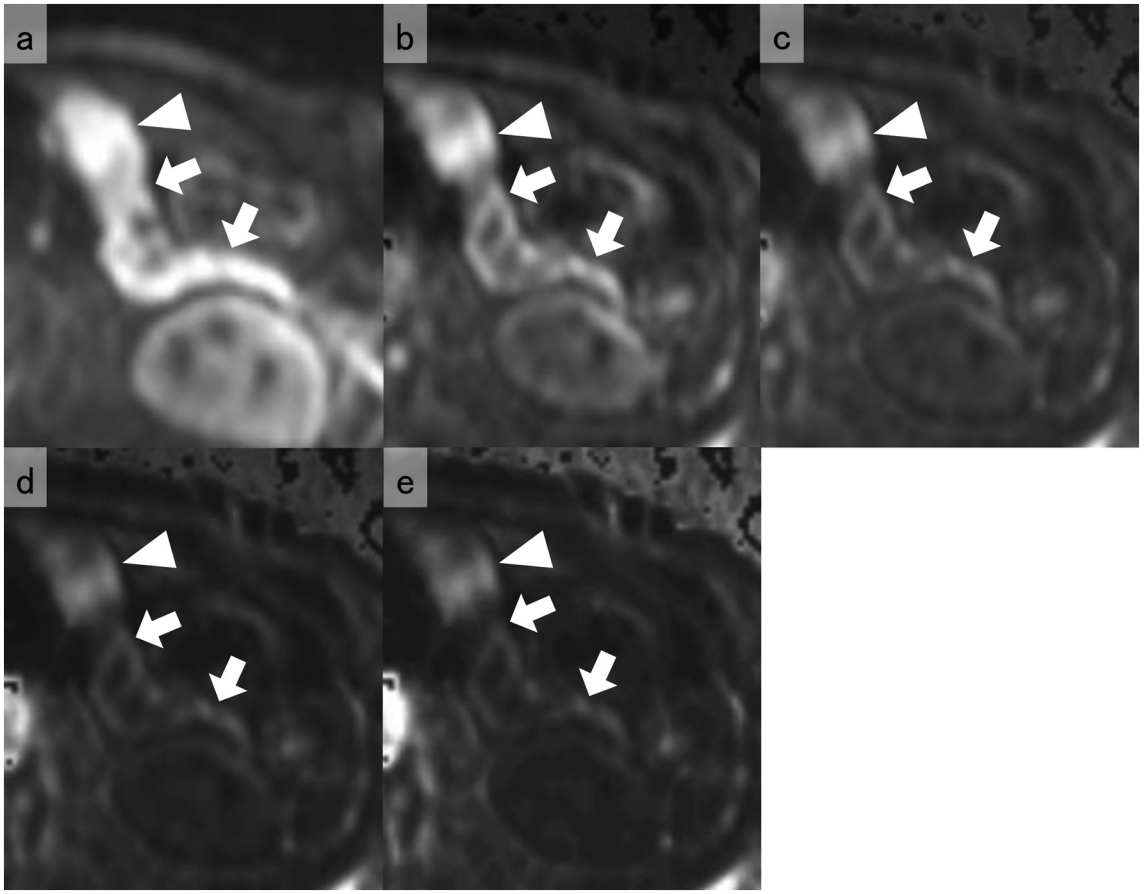

Fig. 1. Diffusion-weighted and computed diffusion-weighted images of pancreatic cancer (arrowheads) and tumor-associated pancreatitis (arrows) in a 65-year-old female patient. Scores for tumor conspicuity/total image quality on (a) DWI_{1000}, (b) $cDWI_{1500}$, (c) $cDWI_{2000}$, (d) $cDWI_{2500}$, and (e) $cDWI_{3000}$ were 2/4, 3/3, 4/2, 4/2, and 4/1, respectively. DWI, diffusion-weighted imaging; cDWI, computed diffusion-weighted imaging.

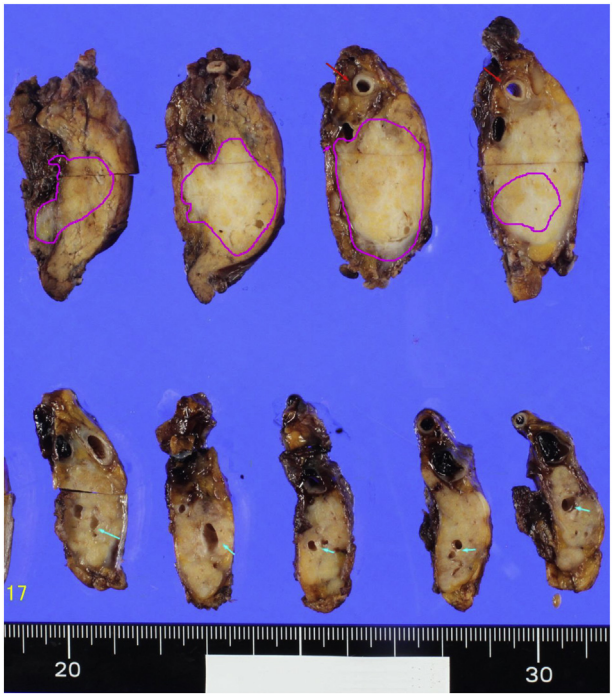

Fig. 2. Pathological cancer map of the sagittal sliced surgical specimen of pancreatic cancer in a 65-year-old female patient (same patient as in Fig. 1). Pink framed areas indicate the cancer. Red and blue arrows represent the bile duct and main pancreatic duct, respectively. (For interpretation of the references to color in this figure legend, the reader is referred to the web version of this article.)

$$V_{Pathology} = \sum (A_{Pathology} \times T_{Pathology}) \quad (5)$$

where $T_{Pathology}$ represents slice thickness of the histopathological specimen.

Volume ratio (VR) of the PC was calculated using the following Eq. (6).

$$VR = V_{DWI}/V_{Pathology} \quad (6)$$

2.7. Statistical analysis

All statistical analyses were performed with commercial software (JMP Pro 13®; SAS Institute, Cary, NC). The Steel test was used to assess tumor conspicuity and total image quality of each cDWI group compared with DWI_{1000}. Student's *t*-test was used to compare ADC values between PC and active TAP. Spearman's rank correlation coefficient was calculated to assess the correlation between ΔADC and tumor conspicuity score on DWI_{1000} and in each cDWI group. The two-one-sided-test was used to assess the equivalency of the PC volume calculated from each cDWI group compared with the pathological specimen in the form of VR. When VR was 1, V_{DWI} and $V_{pathology}$ coincide. Since MRI was performed under respiratory triggering, the range of equivalency was set at 1 ± 0.32 to consider the influence of respiratory fluctuations based on the following Eq. (7):

$$\overline{equivalency} = \frac{1}{n} \sum \left(\frac{V_{Pathology} + R^2 \pi H}{V_{Pathology}} \right) \quad (7)$$

where R, n, and H represent the mean radius of the tumor in the axial plane, the number of cases, and the mean value of respiratory fluctuation in the craniocaudal direction (previously reported as 4 mm [33]), respectively. VR values and the range of equivalency were used in the logarithmic form for analysis. Results were considered statistically significant for values of $P < 0.05$.

Table 2
Patient background characteristics

Age, years [median, (range)]	68 (49–88)
Gender, n (%)	
Male	17 (50.0%)
Female	17 (50.0%)
TNM stage (UICC-7), n (%)	
Stage IA	3 (8.8%)
Stage IB	0 (0%)
Stage IIA	8 (23.6%)
Stage IIB	22 (64.7%)
Stage III	1 (2.9%)
Stage IV	0 (0%)
Location of the PC, n (%)	
Head	21 (61.8%)
Body	11 (32.4%)
Tail	2 (5.8%)
Histology, n (%)	
Adenocarcinoma	
Well differentiated	4 (11.8%)
Moderately differentiated	23 (67.7%)
Poorly differentiated	4 (11.8%)
Adenosquamous carcinoma	1 (2.9%)
Scirrhous carcinoma	2 (5.8%)
Interval between MRI and operation, days [median, (range)]	14 (2 − 30)
Laboratory data within two weeks before MRI, [median (range)]	
Amylase (U/L)	190 (65–502)
Lipase (U/L)	130 (12–1784)
MRI scanner, n (%)	
Magnetom Prisma®	15 (44.1%)
Magnetom Skyra®	19 (55.9%)

UICC-7, TNM classification of malignant tumors 7th edition by Union for International Cancer Control; PC, pancreatic cancer; MRI, magnetic resonance imaging.

3. Results

Based on the inclusion criteria, 79 cases were included. A total of 45 cases were excluded for the following reasons: 42 patients received preoperative therapy; 2 patients were under treatment for another malignant tumor; and 1 patient had pancreatitis associated with endoscopic retrograde cholangiopancreatography based on the medical records. A total of 34 cases were included in the final study. Background characteristics of patients are summarized in Table 2.

As the b-value increased from 1000 to 3000 s/mm^2, tumor conspicuity improved, peaking at a b-value of 2500 s/mm^2 (Fig. 3). Significant improvement in tumor conspicuity was seen with $cDWI_{2000}$ and $cDWI_{2500}$, compared with DWI_{1000} ($P = 0.0121$ and 0.0015, respectively).

Total image quality gradually decreased as the b-value increased (Fig. 4), and all cDWIs showed a significant decrease in total image quality compared with DWI_{1000} ($P < 0.0001$).

PC showed significantly lower ADC values compared with active TAP (mean ± standard deviation of the ADC value: PC, $1.11 \pm 0.19 \times 10^{-3}$ mm^2/s; active TAP, $1.44 \pm 0.29 \times 10^{-3}$ mm^2/s; $P < 0.0001$). Mean value and standard deviation of the ΔADC was $0.33 \pm 0.24 \times 10^{-3}$ mm^2/s.

No significant correlations were seen between ΔADC and tumor conspicuity score on DWI_{1000}. With cDWI, a positive correlation was seen between ΔADC and tumor conspicuity score in all groups. Spearman's rank correlation coefficients were: DWI_{1000}, 0.2797 ($P = 0.1091$); $cDWI_{1500}$, 0.5499 ($P = 0.0008$); $cDWI_{2000}$, 0.6048 ($P = 0.0002$); $cDWI_{2500}$, 0.5086 ($P = 0.0021$); and $cDWI_{3000}$, 0.3790 ($P = 0.0271$) (Fig. 5).

CR increased gradually with increasing b-value (Fig. 6).

VR decreased gradually as the b-value increased, with $cDWI_{2000}$ demonstrating equivalency to the histological specimen ($P = 0.0031$). Other cDWIs were not equivalent to that of the histological specimen

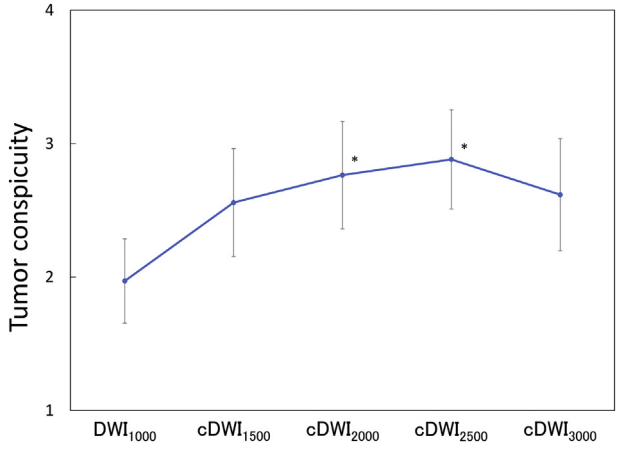

Fig. 3. Line graph of tumor conspicuity of pancreatic cancer within patients with tumor-associated pancreatitis. The blue line represents the mean value, and vertical lines represent standard deviations. *Statistical significance in comparisons between DWI_{1000} with the Steel test. DWI_{1000} vs. $cDWI_{1500}$, $P = 0.0657$; DWI_{1000} vs. $cDWI_{2000}$, $P = 0.0121$; DWI_{1000} vs. $cDWI_{2500}$, $P = 0.0015$; DWI_{1000} vs. $cDWI_{3000}$, $P = 0.0558$. DWI, diffusion-weighted imaging; cDWI, computed diffusion-weighted imaging. (For interpretation of the references to color in this figure legend, the reader is referred to the web version of this article.)

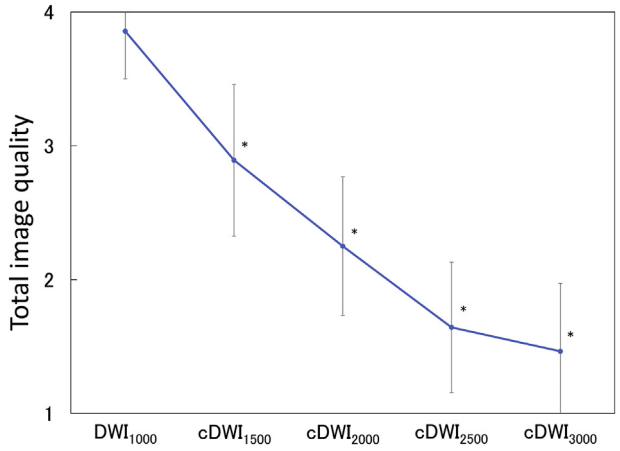

Fig. 4. Line graph of total image quality. The blue line represents the mean value, and vertical lines represent standard deviations. *Statistical significance in comparisons between DWI_{1000} with the Steel test. DWI_{1000} vs. $cDWI_{1500}$, $P < 0.0001$; DWI_{1000} vs. $cDWI_{2000}$, $P < 0.0001$; DWI_{1000} vs. $cDWI_{2500}$, $P < 0.0001$; DWI_{1000} vs. $cDWI_{3000}$, $P < 0.0001$. DWI, diffusion-weighted imaging; cDWI, computed diffusion-weighted imaging. (For interpretation of the references to color in this figure legend, the reader is referred to the web version of this article.)

(Fig. 7).

4. Discussion

DWI allows high visibility of PCs as mass lesions with high SI even when the lesion appears indistinct on dynamic CECT or other MRI sequences, suggesting utility for accurately delineating cancer borders. In the setting of TAP, however, the visibility of PC and the associated border sharpness were lower because both show high SI [8,9].

TAP is an obstructive pancreatitis, occurring from obstruction or stenosis of the main pancreatic duct from mass effect/invasion by the pancreatic tumor [17,34]. TAP consists of several phases of pancreatitis from the acute and active phase to the chronic and inactive phase [17], which show marked differences in the relative proportions of fibrosis,

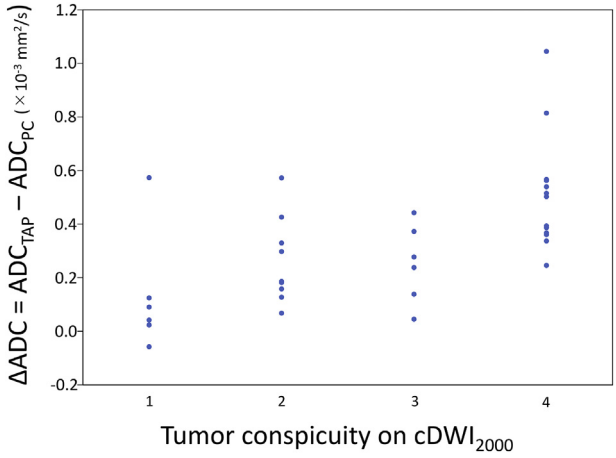

Fig. 5. Scatter plot of ΔADC (ΔADC = ADC_{TAP} − ADC_{PC}) and tumor conspicuity score at $cDWI_{2000}$, with a maximum Spearman's rank correlation coefficient of 0.6048 ($P = 0.0002$). ADC, apparent diffusion coefficient; TAP, tumor-associated pancreatitis; PC, pancreatic cancer; cDWI, computed diffusion-weighted imaging.

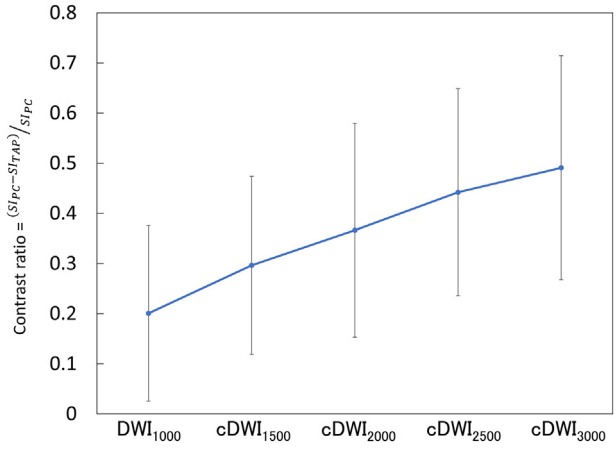

Fig. 6. Line graph of the contrast ratio of PC to TAP. (Contrast ratio = [SI_{PC} − SI_{TAP}] / SI_{PC}). The blue line represents the mean value, and vertical lines represent standard deviations. PC, pancreatic cancer; TAP, tumor-associated pancreatitis; SI, signal intensity; DWI, diffusion-weighted imaging; cDWI, computed diffusion-weighted imaging. (For interpretation of the references to color in this figure legend, the reader is referred to the web version of this article.)

necrosis, and cell density [15]. ADC value of TAP therefore shows a wide range based on the proportion of components [15] and the time course [35,36]. The ADC value of TAP is higher than that of PC in most cases [11,14,37], and the ADC value of active pancreatitis tends to be lower than that of chronic or inactive pancreatitis [15,16]. In our study, active TAP showed slightly but significantly higher ADC values than PC, and mean value of the difference between the two lesions was 0.33. This was consistent with the previous two reports on PC with TAP in which mean difference of ADC values between the two lesions was 0.32–0.38 on DWI with b-values of 0 and 1000 s/mm^2 [14] or 0 and 800 s/mm^2 [37]. Another report on PC with chronic TAP indicated the difference of ADC values between the two lesions as 0.87 on DWI with b-values of 0 and 800 s/mm^2 [11]. With the relatively smaller difference in ADC values between PC and active TAP, distinction between the two lesions is expected on DWI with b-values beyond the usual clinical range.

In the present study, tumor conspicuity in all groups was better with cDWI than with DWI_{1000} with statistical differences at $cDWI_{2000}$ and $cDWI_{2500}$. CR between PC and active TAP increased gradually as the b-

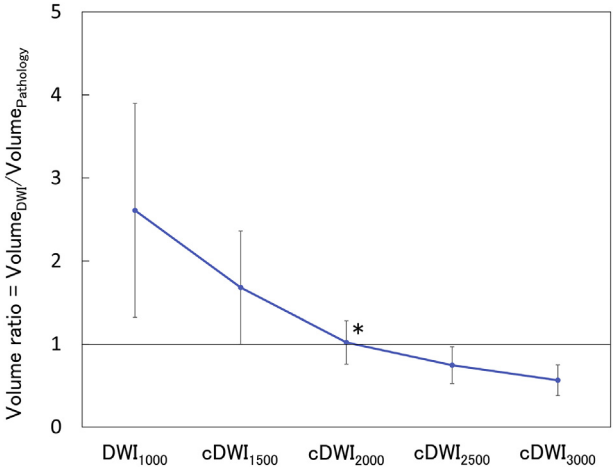

Fig. 7. Line graph of volume ratio of the pancreatic cancer DWI and cDWI with several different b-values (Volume ratio = Volume$_{DWI}$ / Volume$_{Pathology}$). The blue line represents the mean value, and vertical lines represent standard deviations. Horizontal line represents the scale line at the volume ratio of 1. *Statistical significance in the equivalency assessment with the two-one-sided-test compared with the surgical specimen. The range of equivalence was set at 1 ± 0.32. Surgical specimen vs. DWI$_{1000}$, P = 1.000; Surgical specimen vs. cDWI$_{1500}$, P = 0.9517; Surgical specimen vs. cDWI$_{2000}$, P = 0.0031; Surgical specimen vs. cDWI$_{2500}$, P = 0.7554; Surgical specimen vs. cDWI$_{3000}$, P = 0.9999. DWI, diffusion-weighted imaging; cDWI, computed diffusion-weighted imaging. (For interpretation of the references to color in this figure legend, the reader is referred to the web version of this article.)

value increased. Moreover, all cDWI groups demonstrated significant positive correlations between ΔADC and tumor conspicuity, with the largest correlation coefficient seen for cDWI$_{2000}$. The difference in SIs between the two lesions was emphasized in the cDWI with higher b-value by the difference in ADC values. SI of active TAP decreased more rapidly than that of PC as the b-value increased, so cDWI with the higher b-value induced larger contrast between the two lesions. If the b-value was set too high, however, tumor conspicuity decreased despite an increasing CR, possibly due to overall decreases in total image quality. DWI$_{1000}$ presented the best total image quality, and it decreased gradually while the b-value increased. This trend corresponds to several previous reports [19,21,23]. The higher b-value induces higher signal suppression and lower SIs in pixels based on the mathematical model [21] leading to a lower signal-to-noise ratio and obscuring the anatomical orientation. Increases in noise with increasing b-value could be another reason for the decreasing trend in total image quality [38].

In a previous study of PC detection with cDWI, the best tumor detectability was achieved with cDWI$_{1500}$ [23]. This study included all PC patients without any information about the presence or absence of TAP. In PC patients with active TAP, the difference in ADC values between the two lesions became small. In these cases, the cDWI with higher b-value (such as cDWI$_{2000}$ or cDWI$_{2500}$) was more suitable, particularly for evaluation of the border between PC and active TAP.

The area of high SI on DWI$_{1000}$ was larger than the actual area of the PC. We suggest this was caused by not only active TAP, which migrates the seeming border of the PC to the upstream side, but also the microscopic pancreatitis that occurs around the PC from occlusion of the small branches of the peritumoral pancreatic duct [17]. Conversely, cDWI$_{3000}$ showed a high-SI area smaller than the actual area of the PC. When the b-value increases, part of the PC may become difficult to recognize as a high SI area because of its histologic heterogeneity [39,40]. In our study, the volume on cDWI$_{2000}$ demonstrated the closest and equivalent volume with statistical significance compared with the surgical specimen. Use of cDWI$_{2000}$ might delineate most parts of PC as high SI, while minimizing false-positive findings from active TAP and peritumoral pancreatitis, although this remains speculative under the lack of precise correlations between image and pathology in each case. Considering the results of volume in addition to the qualitative evaluation, cDWI$_{2000}$ was the optimal b-value for clear and accurate depiction in PC patients with coexisting active TAP.

Among our cases, three demonstrated low tumor conspicuity (score 1) in the qualitative evaluation on DWI$_{1000}$ with no improvement in scores among cDWI sets. ΔADC in these cases (−0.06, 0.04, and 0.09) were some of the smallest ΔADCs among our cases. The ADC value of TAP has a range as mentioned above, so the ADC value of active TAP can take a similar or lower value than that of PC, as described in a previous report [9]. In these cases, SI of PC decreases as fast or faster than the active TAP as the b-value increases, resulting in low visibility of the PC. Except in such specific cases, cDWI with high b-value was useful and accurate regarding the tumor border in most patients. Adding cDWI with a high b-value to routine clinical MRI practice can be achieved without any additional burden on patients, including total scan time of MRI, since cDWI is available retrospectively. In addition, cDWI may have the potential to contribute to abbreviated MRI thanks to its use of post-examination processing.

Several limitations to our study must be considered. First, the number of patients was restricted because of the advanced disease, resulting in many patients undergoing neoadjuvant chemo-radiotherapy or being deemed inoperable. Second, in this study, the cDWI used was generated from two b-values of 0 and 1000 s/mm^2 based on previous studies. The results of cDWI created using other combinations of the b-values have not been examined. Third, the existence and activity of TAP was not confirmed pathologically. Fourth, because of the retrospective nature of the study, data on directly measured DWI$_{1500}$–DWI$_{3000}$ were lacking.

5. Conclusion

In patients with PC and active TAP, adding cDWI with high b-value could be useful for clearly distinguishing between PC and active TAP. In these patients, cDWI with a b-value of 2000 s/mm^2 was optimal when evaluating images regarding tumor conspicuity, total image quality, and tumor volume.

Funding disclosures

This research did not receive any specific grant from funding agencies in the public, commercial, or not-for-profit sectors.

Declaration of competing interest

The authors declare that they have no conflict of interest.

Acknowledgements

We acknowledge Shigeshi Kohno, MD and Toshiyuki Sato, MD from Kyoto University Graduate School of Medicine, Department of Diagnostic Imaging and Nuclear Medicine, for image evaluation, and Tosiya Sato, PhD from Kyoto University School of Public Health, Department of Biostatistics, for statistical advice and revision of the manuscript.

References

[1] Siegel R, Ward E, Brawley O, Jemal A. Cancer statistics, 2011: the impact of eliminating socioeconomic and racial disparities on premature cancer deaths. CA Cancer J Clin 2011;61:212–36. https://doi.org/10.3322/caac.20121.

[2] Arvold ND, Niemierko A, Mamon HJ, Fernandez-del Castillo C, Hong TS. Pancreatic cancer tumor size on CT scan versus pathologic specimen: implications for radiation treatment planning. Int J Radiat Oncol Biol Phys 2011;80:1383–90https://doi.org/10.1016/j.ijrobp.2010.04.058.

[3] Caravatta L, Sallustio G, Pacelli F, et al. Clinical target volume delineation including

elective nodal irradiation in preoperative and definitive radiotherapy of pancreatic cancer. Radiat Oncol 2012;7(86)https://doi.org/10.1186/1748-717x-7-86.
[4] Dalah E, Moraru I, Paulson E, Erickson B, Li XA. Variability of target and normal structure delineation using multimodality imaging for radiation therapy of pancreatic cancer. Int J Radiat Oncol Biol Phys 2014;89:633–40https://doi.org/10.1016/j.ijrobp.2014.02.035.
[5] Cassinotto C, Mouries A, Lafourcade JP, et al. Locally advanced pancreatic adenocarcinoma: reassessment of response with CT after neoadjuvant chemotherapy and radiation therapy. Radiology 2014;273:108–16https://doi.org/10.1148/radiol.14132914.
[6] Lambrecht M, Dirix P, Vandecaveye V, De Keyzer F, Hermans R, Nuyts S. Role and value of diffusion-weighted MRI in the radiotherapeutic management of head and neck cancer. Expert Rev Anticancer Ther 2010;10:1451–9https://doi.org/10.1586/era.10.121.
[7] Schima W, Ba-Ssalamah A, Kolblinger C, Kulinna-Cosentini C, Puespoek A, Gotzinger P. Pancreatic adenocarcinoma. Eur Radiol 2007;17:638–49https://doi.org/10.1007/s00330-006-0435-7.
[8] Kartalis N, Lindholm TL, Aspelin P, Permert J, Albiin N. Diffusion-weighted magnetic resonance imaging of pancreas tumours. Eur Radiol 2009;19:1981–90. https://doi.org/10.1007/s00330-009-1384-8.
[9] Fukukura Y, Takumi K, Kamimura K, et al. Pancreatic adenocarcinoma: variability of diffusion-weighted MR imaging findings. Radiology 2012;263:732–40https://doi.org/10.1148/radiol.12111222.
[10] Shinya S, Sasaki T, Nakagawa Y, Guiquing Z, Yamamoto F, Yamashita Y. Usefulness of diffusion-weighted imaging (DWI) for the detection of pancreatic cancer: 4 case reports. Hepatogastroenterology 2008;55:282–5.
[11] Matsuki M, Inada Y, Nakai G, et al. Diffusion-weighed MR imaging of pancreatic carcinoma. Abdom Imaging 2007;32:481–3https://doi.org/10.1007/s00261-007-9192-6.
[12] Ichikawa T, Erturk SM, Motosugi U, et al. High-b value diffusion-weighted MRI for detecting pancreatic adenocarcinoma: preliminary results. AJR Am J Roentgenol 2007;188:409–14https://doi.org/10.2214/ajr.05.1918.
[13] White NS, McDonald C, Farid N, et al. Diffusion-weighted imaging in cancer: physical foundations and applications of restriction spectrum imaging. Cancer Res 2014;74:4638–52https://doi.org/10.1158/0008-5472.Can-13-3534.
[14] Huang WC, Sheng J, Chen SY, Lu JP. Differentiation between pancreatic carcinoma and mass-forming chronic pancreatitis: usefulness of high b value diffusion-weighted imaging. J Dig Dis 2011;12:401–8https://doi.org/10.1111/j.1751-2980.2011.00517.x.
[15] Barral M, Taouli B, Guiu B, et al. Diffusion-weighted MR imaging of the pancreas: current status and recommendations. Radiology 2015;274:45–63https://doi.org/10.1148/radiol.14130778.
[16] Nam IC, Kim SH, Kim SJ, Lim YJ. Added value of diffusion weighted imaging for detecting pancreatic abnormality in patients with clinically suspected acute pancreatitis. Investig Magn Reson Imaging 2016;20:241–9https://doi.org/10.13104/imri.2016.20.4.241.
[17] Inoue T. A histopathological study of 60 autopsied cases of primary pancreatic carcinoma with reference to pathogenesis of the tumor concomitant pancreatitis. Juntendo Med J 1976;22:62–90 [in Japanese, English abstract available].
[18] Fukukura Y, Shindo T, Hakamada H, et al. Diffusion-weighted MR imaging of the pancreas: optimizing b-value for visualization of pancreatic adenocarcinoma. Eur Radiol 2016;26:3419–27https://doi.org/10.1007/s00330-015-4174-5.
[19] Rosenkrantz AB, Oei M, Babb JS, Niver BE, Taouli B. Diffusion-weighted imaging of the abdomen at 3.0 tesla: image quality and apparent diffusion coefficient reproducibility compared with 1.5 tesla. J Magn Reson Imaging 2011;33:128–35https://doi.org/10.1002/jmri.22395.
[20] Schmid-Tannwald C, Oto A, Reiser MF, Zech CJ. Diffusion-weighted MRI of the abdomen: current value in clinical routine. J Magn Reson Imaging 2013;37:35–47https://doi.org/10.1002/jmri.23643.
[21] Blackledge MD, Leach MO, Collins DJ, Koh DM. Computed diffusion-weighted MR imaging may improve tumor detection. Radiology 2011;261:573–81https://doi.org/10.1148/radiol.11101919.
[22] Rosset A, Spadola L, Ratib O. OsiriX: an open-source software for navigating in multidimensional DICOM images. J Digit Imaging 2004;17:205–16. https://doi.org/10.1007/s10278-004-1014-6.
[23] Fukukura Y, Kumagae Y, Hakamada H, et al. Computed diffusion-weighted MR imaging for visualization of pancreatic adenocarcinoma: comparison with acquired diffusion-weighted imaging. Eur J Radiol 2017;95:39–45https://doi.org/10.1016/j.ejrad.2017.07.022.
[24] Bollen TL, Singh VK, Maurer R, et al. Comparative evaluation of the modified ct severity index and CT severity index in assessing severity of acute pancreatitis. AJR Am J Roentgenol 2011;197:386–92https://doi.org/10.2214/ajr.09.4025.
[25] Li S, Tian B. Acute pancreatitis in patients with pancreatic cancer: timing of surgery and survival duration. Medicine (Baltimore) 2017;96:e5908https://doi.org/10.1097/md.0000000000005908.
[26] Shimizu H, Isoda H, Fujimoto K, et al. Comparison of acquired diffusion weighted imaging and computed diffusion weighted imaging for detection of hepatic metastases. Eur J Radiol 2013;82:453–8https://doi.org/10.1016/j.ejrad.2012.10.020.
[27] Tokunaga K, Arizono S, Isoda H, Shimizu H, Fujimoto K, Togashi K. Optimal combinations of b-values in computed DWI for pancreatic cancer detection. Annual meeting International Society of Magnetic Resonance Imaging 2018. 2018https://cds.ismrm.org/protected/18MPresentations/abstracts/4706.html [Accessed 7 November 2018].
[28] Le Bihan D, Breton E. Imagerie de diffusion in vivo par résonance magnétique nucléaire. C R Acad Sci II 1985;301:1109–12.
[29] Takahara T. Developing a computed DWI application for ziostation 2. Innervision 2014;29:111–4. [in Japanese].
[30] Kang KM, Lee JM, Yoon JH, Kiefer B, Han JK, Choi BI. Intravoxel incoherent motion diffusion-weighted MR imaging for characterization of focal pancreatic lesions. Radiology 2014;270:444–53https://doi.org/10.1148/radiol.13122712.
[31] Klauss M, Lemke A, Grunberg K, et al. Intravoxel incoherent motion MRI for the differentiation between mass forming chronic pancreatitis and pancreatic carcinoma. Invest Radiol 2011;46:57–63https://doi.org/10.1097/RLI.0b013e3181fb3bf2.
[32] Malone SC, Haridass A, Nyiri B, et al. Creation of 3-dimensional prostate cancer maps: methodology and clinical and research implications. Arch Pathol Lab Med 2014;138:803–8https://doi.org/10.5858/arpa.2012-0609-OA.
[33] Jayachandran P, Minn AY, Van Dam J, Norton JA, Koong AC, Chang DT. Interfractional uncertainty in the treatment of pancreatic cancer with radiation. Int J Radiat Oncol Biol Phys 2010;76:603–7https://doi.org/10.1016/j.ijrobp.2009.06.029.
[34] Gabata T, Sanada J, Kobayashi S, Terayama N, Kadoya M, Matsui O. Tumor-associated focal chronic pancreatitis from invasion of the pancreatic duct by common bile duct carcinoma: radiologic-pathologic correlation. Abdom Imaging 2003;28:378–80https://doi.org/10.1007/s00261-002-0049-8.
[35] Shinya S, Sasaki T, Nakagawa Y, Guiquing Z, Yamamoto F, Yamashita Y. Acute pancreatitis successfully diagnosed by diffusion-weighted imaging: a case report. World J Gastroenterol 2008;14:5478–80.
[36] Thomas S, Kayhan A, Lakadamyali H, Oto A. Diffusion MRI of acute pancreatitis and comparison with normal individuals using ADC values. Emerg Radiol 2012;19:5–9https://doi.org/10.1007/s10140-011-0983-2.
[37] Hayano K, Miura F, Wada K, et al. Diffusion-weighted MR imaging of pancreatic cancer and inflammation: prognostic significance of pancreatic inflammation in pancreatic cancer patients. Pancreatology 2016;16:121–6https://doi.org/10.1016/j.pan.2015.10.004.
[38] Kwee TC, Takahara T, Ochiai R, Nievelstein RA, Luijten PR. Diffusion-weighted whole-body imaging with background body signal suppression (DWIBS): features and potential applications in oncology. Eur Radiol 2008;18:1937–52. https://doi.org/10.1007/s00330-008-0968-z.
[39] Muraoka N, Uematsu H, Kimura H, et al. Apparent diffusion coefficient in pancreatic cancer: characterization and histopathological correlations. J Magn Reson Imaging 2008;27:1302–8https://doi.org/10.1002/jmri.21340.
[40] Lee SS, Byun JH, Park BJ, et al. Quantitative analysis of diffusion-weighted magnetic resonance imaging of the pancreas: usefulness in characterizing solid pancreatic masses. J Magn Reson Imaging 2008;28:928–36https://doi.org/10.1002/jmri.21508.